JOURNAL OF GEOPHYSICAL RESEARCH, VOL. 106, NO. A11, PAGES 25,451-25,465, NOVEMBER 1, 2001

Global hybrid simulation of the dayside reconnection layer and associated field-aligned currents

Y. Lin

Physics Department, Auburn University, Auburn, Alabama, USA

Abstract. A two-dimensional global hybrid simulation is carried out to study the structure of the magnetopause boundary layer in the noon-midnight meridian plane associated with the dayside reconnection. In the simulation the bow shock, magnetosheath, and magnetopause are formed self-consistently by supersonic solar wind passing the geomagnetic field. The dayside reconnection is triggered by imposing a current-dependent resistivity at the subsolar magnetopause. A large-amplitude rotational discontinuity is formed in the quasi-steady reconnection layer in the northern and southern hemispheres. The rotational discontinuity possesses an electron sense, or right-hand polarization in the magnetic field as the discontinuity is formed from the X line, and the magnetic structures in the magnetopause northward and southward of the X line are asymmetric in the cases with a nonzero B_y component of the interplanetary magnetic field (IMF). However, later the rotational discontinuity tends to evolve to a structure with a smallest field rotational angle and thus may reverse its sense of the field rotation. The Walén relation is tested for electron and ion flows in the magnetopause rotational discontinuities with left-hand and right-hand polarizations. Field-aligned currents are generated in the magnetopause rotational discontinuity during the reconnection, and nearly 5% of the magnetopause currents propagate with Alfvén waves along the field lines into the polar ionosphere. In addition, a weak secondary rotational discontinuity or Alfvén wave pulse propagates from the reconnection site into the magnetosphere. The sense of the field-aligned currents is investigated for various values of the IMF B_y. The Hall effects on the structure of the magnetopause boundary layer and the field-aligned currents are discussed.

1. Introduction

Reconnection of magnetic field lines from the magnetosheath and the magnetosphere can take place at the magnetopause where an antiparallel magnetic field component is present across the magnetopause current sheet. Magnetic reconnection is believed to be one of the most important mechanisms for the transfer of the mass, momentum, and energy from the solar wind to the Earth's magnetosphere [*Dungey*, 1961; *Vasyliunas*, 1975]. Transient reconnection events such as the flux transfer events (FTEs) have often been observed at the magnetopause [e.g., *Russell and Elphic*, 1978].

Quasi-steady magnetic reconnection generates an outflow region known as the magnetic reconnection layer. Theoretical models show that various types of MHD discontinuities may exist in the dayside reconnection layer [*Levy et al.*, 1964; *Heyn et al.*, 1988; *Lin and Lee*, 1994a], including rotational discontinuities, slow shocks, and slow expansion waves. A large-amplitude rotational discontinuity, through which the magnetic field changes its direction from the magnetosheath to the magnetosphere, at the magnetopause and the associated flow acceleration/deceleration due to the magnetic tension force have indeed been found in many satellite observations at the subsolar magnetopause [*Paschmann et al.*, 1979; *Sonnerup et al.*, 1981; *Nakamura et al.*, 1996], the high-latitude magnetopause [*Gosling et al.*, 1991; *Kessel et al.*, 1996; *Scudder et al.*, 1999; *Fuselier et al.*, 2000; *Russell et al.*, 2000], and the flanks of the magnetopause [*Gosling et al.*, 1986]. A slow expansion fan-like structure is found to be attached to the magnetopause rotational discontinuity on the magnetospheric side. The existence of the rotational discontinuity and the associated flow acceleration have been considered major evidence for the occurrence of magnetic reconnection at the magnetopause. Slow shocks, however, have seldom been observed at the magnetopause because of the free ion mixing along the field lines [*Lin and Lee*, 1994a]. Recent observations by *Phan et al.* [2000] provide strong evidence for the existence of a stable extended equatorial X line along the dayside magnetopause during periods of strongly southward interplanetary magnetic field (IMF).

Paper number 2000JA000184.
0148-0227/01/2000JA000184$09.00

Theoretical studies also indicate that there, in general, exist two rotational discontinuities in the reconnection layer [e.g., *Lin and Lee*, 1994a]. In addition to the primary magnetopause rotational discontinuity, which is hereinafter referred to as RD1, there may be a secondary rotational discontinuity, referred to as RD2, or Alfvén wave propagating on the magnetospheric side. Near the subsolar region, the strength of RD2 is much weaker than that of RD1 and decreases with the ion density on the magnetospheric side of the magnetopause boundary layer.

The structure of the dayside reconnection layer has been studied in one-dimensional (1-D) simulations of the Riemann problem [*Lin and Lee*, 1994a, 1994b; *Omidi and Winske*, 1995] and two-dimensional (2-D) MHD [*Scholer*, 1989; *Shi and Lee*, 1990; *Lin and Lee*, 1999] and hybrid [*Lin and Xie*, 1997; *Krauss-Varban et al.*, 1999; *Nakamura and Scholer*, 2000; *Xie and Lin*, 2000] simulations. In these 2-D simulations of the reconnection, however, the simulation domain contains only a small portion of the magnetopause near the reconnection X line, and the magnetosheath and the magnetospheric conditions are chosen artificially.

In this paper, we present the first 2-D global hybrid simulation of the structure of the dayside reconnection layer associated with quasi-steady reconnection, which corresponds to an extended reconnection X line along the equatorial magnetopause [e.g., *Phan et al.*, 2000]. Although there have been global simulations of dayside reconnection using MHD or hybrid particle models [e.g., *Ogino et al.*, 1986; *Fedder and Lyon*, 1987; *Omidi et al.*, 1998], the structure of discontinuities in the magnetopause boundary layer on the global scale has not been investigated in kinetic simulations. In our simulation the bow shock, the magnetosheath, and the magnetosphere form self-consistently. The effects of a finite B_y component in the interplanetary magnetic field (IMF) are simulated.

The sense of the field rotation through the magnetopause rotational discontinuity determines the sense of field-aligned currents generated at the magnetopause current layer. It was suggested by *Lee et al.* [1985], *Saunders* [1989], and *Lin and Lee* [1994c] that the leakage of the field-aligned currents from the magnetopause rotational discontinuities or Alfvén waves can lead to the generation of traditional cusp/mantle field-aligned current system. Observations at the magnetopause by *Sonnerup and Cahill* [1968] indicated that the sense of the magnetic field rotation across the magnetopause may depend on the normal component of the field and is in opposite sense above and below the magnetic equator. On the other hand, observations by *Berchem and Russell* [1982] showed that the magnetic field rotates from the magnetosheath direction to the magnetospheric direction by the shortest angular path. While most of satellite magnetopause crossings show that the magnetic field rotation follows the shortest path through rotational discontinuities, a large field rotation of ~195° appeared in the rotational discontinuity observed by a magnetopause crossing of OGO 5 [*Sonnerup and Ledley*, 1979]. An example of >270° field rotation was also found at the Uranian magnetopause [*Russell et al.*, 1989]. Satellite observations also indicate that field-aligned currents are carried by Alfvén waves along magnetic flux tubes of reconnection [*Saunders et al.*, 1984]. MHD simulations [e.g., *Sato et al.*, 1984; *Scholer and Otto*, 1991; *Ma et al.*, 1995; *Ma and Lee*, 1999] show the generation of field-aligned currents by reconnection in the magnetotail or transient reconnection at the magnetopause. In this paper, the generation of field-aligned currents at rotational discontinuities in collisionless plasmas and their propagation to the high-latitude ionosphere are investigated on a global scale.

The outline of the paper is as follows. The simulation model is given in section 2. The simulation results of the dayside reconnection are shown in section 3. Finally, a summary is given in section 4.

2. Simulation Model

The 2-D ($\partial/\partial y = 0$) simulation is carried out in the noon-midnight meridian plane, in which the x axis is assumed to be along the Sun-Earth line and pointing to the Sun, and the z axis is pointing from the south to the north. A polar coordinate system is used in the simulation; this system consists of the radial distance r in the xz plane and the polar angle $\theta \equiv \tan^{-1}(x/z)$. The Earth is located at the origin $(x, z) = (0, 0)$. The simulation domain is within the region with $1\ R_E < r < 24\ R_E$ and $0° \le \theta \le 180°$. The inner boundary at $r = 1\ R_E$ corresponds to the surface of the Earth.

The 2-D hybrid code adapted in this study was developed by *Swift* [1996]. In the hybrid code the ions (protons) are treated as discrete particles, and the electrons are treated as a massless fluid. Quasi-charge neutrality is guaranteed in the simulation. The equation for ion motion is given by

$$\frac{d\mathbf{v}_i}{dt} = \mathbf{E} + \mathbf{v}_i \times \mathbf{B} - \nu(\mathbf{V}_i - \mathbf{V}_e), \tag{1}$$

where $\mathbf{v}_i$ is the ion particle velocity, $\mathbf{E}$ is the electric field in units of ion acceleration, $\mathbf{B}$ is the magnetic field in units of the ion gyrofrequency, ν is the collision frequency which is used to model the resistivity at the X line, and $\mathbf{V}_e$ and $\mathbf{V}_i$ are the bulk flow velocities of electrons and ions, respectively. The particles are advanced at exact spatial locations, while the field quantities, the number densities, and the velocity moments are calculated at cell grids. The ion bulk flow velocity at each cell grid is calculated by summing weighted particle velocities around the grid. The electron momentum equation for a zero electron pressure is written in the form

$$\mathbf{E} = -\mathbf{V}_e \times \mathbf{B} - \nu(\mathbf{V}_e - \mathbf{V}_i). \tag{2}$$

The electron flow speed is evaluated from Ampere's law,

$$\mathbf{V}_e = \mathbf{V}_i - \frac{\nabla \times \mathbf{B}}{\alpha N}, \quad (3)$$

where the charge coupling constant $\alpha = (4\pi e^2/m_i c^2)$, e is the electron charge, m_i is the ion mass, and N is the ion number density. The magnetic field is advanced in time from Faraday's law

$$\frac{\partial \mathbf{B}}{\partial t} = -\nabla \times \mathbf{E}, \quad (4)$$

where the electric field is calculated from (2).

The ion gyrofrequency Ω_0 in the solar wind is chosen to be 1.0 s^{-1}, where $\Omega_0 = eB_0/m_i$, and B_0 is the magnitude of the IMF. This value of Ω_0 corresponds to an IMF $B_0 \sim 10$ nT. The number of ion particles per R_E^2 in the solar wind is chosen to be $N_0 = 1000$. In the calculation the charge coupling constant α is chosen as a scaling parameter. The ion inertial length $\lambda_0 \equiv c/\omega_{pi0} = 1/\sqrt{N_0\alpha}$, where ω_{pi0} is the ion plasma frequency, is chosen to be 0.16 R_E. The Alfvén speed in the solar wind is $V_{A0} = 0.16\ R_E s^{-1}$. The ion plasma beta is chosen to be $\beta_0 = 0.5$ in the solar wind. Note that the above values of the ion inertial length and the Alfvén speed are 10 times the values in the real solar wind. These values are chosen to accommodate realistic computing resources. In our simulation a total of 2,000,000 particles is used. We have also run the simulation for a smaller value of λ_0 and found that the structure of the bow shock and the magnetopause are nearly unchanged when scaled to the ion inertial length and the Alfvén speed.

In our simulation the grids are uniformly distributed in the θ directions for each radial shell, with a total of 142 grid points. Nonuniform grid sizes Δr are used in the r direction, with denser grids near the magnetopause boundary region. The grid size $\Delta r \simeq 0.05\ R_E$ from $r = 9.5\ R_E$ to 12.5 R_E, while in other areas, Δr is also less than the local ion inertial length. The time step of particle advance is $\Delta t = 0.02\Omega_0^{-1}$. The advances of particle velocities and magnetic field are accurate to second order in both time and space [*Swift*, 1996]. The most serious source of errors arises from the finite particle number n per cell, which causes the fluctuations of physical quantities by an amplitude of $\sim 1/\sqrt{n}$ on the scale of grid size. About 100-200 particles are used in each cell in the magnetosheath and the magnetopause to assure a reasonable statistical results. In addition, the conservation of total energy in the simulation domain is also checked, and it is also accurate to second order in time.

Initially, the solar wind density and the IMF are assumed to be uniform in $r > 10\ R_E$. The z component of the IMF is negative (southward), and a finite y component IMF, B_{y0}, is also assumed. A 2-D dipole field plus an image dipole occupies the geomagnetic region with $r < 10\ R_E$. The dipole moment corresponds to a magnetic field of 50 nT at the magnetopause. An initial particle density of $\sim 200\ R_E^{-2}$ is assumed on the magnetospheric side of the magnetopause. The initial ion temperature is assumed to be isotropic, with $T_{m0} = 100T_0$, where T_{m0} and T_0 are the initial temperatures in the magnetosphere and the solar wind, respectively. In addition to the ion particle dynamics described above, a cold, dense fluid population occupies the magnetospheric region of $r < 6\ R_E$ to represent the dense plasma in the inner magnetosphere [*Swift*, 1996]. Since the electron temperature is much less than the ion temperature in the magnetosheath and the magnetosphere, in our study the electron temperature is assumed to be zero for simplicity. Recent particle and Hall-MHD simulations indicate that the reconnection rate is insensitive to the triggering mechanisms, in which the electrons play an important role, that break the frozen-in condition [e.g., *Shay et al.*, 2001]. While the structure near the X line is on the scale of electron inertial length, the structure of the outflow region is dominated by the ion physics on the scale of the ion inertial length. Previous simulations also show that the overall structure of the magnetopause rotational discontinuity is nearly not affected by the electron temperature and a small resistivity [e.g., *Lee et al.*, 1989].

The inflow speed V_0 of the solar wind is assumed to correspond to the magnetosonic Mach number $M_A \equiv V_0/V_{A0} = 5$. In the simulation the solar wind flows along the $-x$ direction from the front side semicircular boundary at $r = 24\ R_E$ and convects the IMF $\mathbf{B}_0$ into the simulation domain. Outflow boundary conditions are used at the two straight-line polar axes at $\theta = 0°$ (north) and $\theta = 180°$ (south). The bow shock, the magnetosheath, and the magnetopause boundary are formed first by the interaction between the supersonic solar wind and the magnetopause, and then a current-dependent collision frequency is imposed at the region with $|r - 10\ R_E| < 1.5\ R_E$ and $|\theta - 90°| < 1.3°$ in the subsolar magnetopause current sheet to trigger the reconnection. No resistivity is applied for other regions in the simulation domain. The collision frequency ν near the subsolar magnetopause is given by

$$\nu = 0.04\Omega_0 |J(r,\theta)/J_0|, \quad (5)$$

where J is the electric current density and $J_0 \equiv B_0/(\mu_0\lambda_0)$. In the simulation the average value ν at the subsolar magnetopause is $0.15\Omega_s$, where Ω_s is the ion gyrofrequency in the magnetosheath region just outside the magnetopause. The study conducted in this paper corresponds to a single, long X line along y. For most of the cases shown in this paper the initial half width of the magnetopause current sheet is 0.1 R_E. A case with a much thinner magnetopause is also shown. The ion collision frequency is 0.1-1 ion gyrofrequency in the magnetosheath, and thus the Lundquist number based on the magnetosheath Alfvén speed and the ion inertial length is ~1-10. A perfect conducting boundary is assumed at the ionospheric boundary at $r = 1\ R_E$. Our study will concentrate on the physics of the magne-

topause boundary layer. The effects of the ionosphere on the magnetopause currents will not be discussed in this paper.

The normalization of physical quantities in the presentation is as follows. The magnetic field B is normalized to the IMF B_0, the ion number density N is normalized to the solar wind density N_0, the flow velocity V is normalized to V_{A0}, and the time t is normalized to Ω_0^{-1}. The spatial coordinates are expressed in units of R_E. The electric current density J is normalized to J_0.

3. Structure of the Magnetopause Reconnection Layer and Generation of Field-Aligned Currents

We show the simulation results of five cases. In case 1 the IMF $B_{y0} = 0$. In cases 2, 3, and 5, $B_{y0} > 0$. Results for $B_{y0} < 0$ are shown in case 4. Note that in the 2-D simulation the B_z component of the magnetic field piles up in front of the subsolar magnetopause before being removed by the reconnection, while the B_y component convects away with the flow velocity V_z. Therefore, in the cases with $B_{y0} \neq 0$ the ratio between the B_y and B_z in the magnetosheath in our 2-D model is smaller than that in the 3-D situation.

Figure 1 (left) shows the results of case 1 at $t = 40\Omega_0^{-1}$. Figure 1a shows the magnetic field lines in the xz plane plotted on top of the contours of the field magnitude B in the logarithm scale. Figures 1b and 1c show the contours of B_y component and ion number density N, respectively. Figure 1d shows the ion flow vectors and the contours of the ion flow speed in the xz plane. Figure 1e shows the contours of the field-aligned current density $J_\parallel$. All the contour plots are in gray scales, with the black representing the maximum contour levels plotted and the white representing the minimum levels. For B_y and $J_\parallel$, the dark shading represents positive values and and the light shading represents the negative values. The heavy semicircles at $r = 1\ R_E$ and 24 R_E mark the boundaries of the simulation domain.

An X line has formed near the subsolar magnetopause at $r \sim 10\ R_E$, and the reconnected field lines are carried northward and southward by the plasma flow. Two transient plasmoids (closed field line loops) are seen in the northern and the southern hemispheres, as shown in the field line plot. The bow shock occurs at a standoff distance of $\sim$18 R_E, across which the magnetic field is enhanced and the flow turns to the latitudinal directions around the magnetopause. The half width of the magnetopause current layer is $3\lambda_s$ near the subsolar region, where λ_s is the ion inertial length in the magnetosheath just in front of the magnetopause, but is much larger in the plasmoid regions. Behind the plasmoids, negative and positive B_y fluctuations are present in the northern and the southern magnetopause boundary layers, respectively. The presence of the finite B_y oscillations is due to the Hall effects associated with the finite ion Larmor radii [*Sonnerup*, 1979]. In the opened magnetopause regions, where the magnetospheric field lines are connected with the magnetosheath field lines, the incident ions and electrons from the magnetosheath can penetrate across the magnetopause. Considering that the ion mass is much larger than the electron mass, we can ignore the electron inertial effects. In the boundary layer region the field lines have a radius of curvature comparable with the ion Larmor radii, and the incident ions are slowed down and lag behind the electrons. This finite ion Larmor radius effect results in a negative and positive $J_\parallel$ in the northern and southern hemispheres, respectively. The Hall current loops in the xz plane result in a finite B_y. The maximum B_y in the current layer can be estimated as

$$B_y \simeq \mu_0 J_\parallel \Delta, \tag{6}$$

where Δ is the width of the magnetopause current layer. As seen from the $J_\parallel$ contours, the negative and positive parallel currents exist throughout the northern and southern current layers, respectively, in which the field lines are twisted. These current layers behind the leading plasmoids are essentially a rotational discontinuity (large-amplitude Alfvén wave) whose upstream is on the magnetosheath side, as to be discussed below. The Hall currents and the associated B_y structure discussed here are present at the kinked field lines, which convect with the plasma outflows ejected by the magnetic tension force, in the reconnection layer. Since the particle density in the magnetosphere is much less than that in the magnetosheath, the B_y and $J_\parallel$ patterns in the magnetopause are dominated by the Hall effects associated with the magnetosheath particles. The Hall effects associated with the finite ion inertia, or the dispersive structures, of discontinuities or laminar shock waves may be obtained by two-fluid models [e.g., *Tidman and Krall*, 1971; *Lyu and Kan*, 1989], but the Hall-MHD models are only approximately corresponding to the situation when ion β approaches zero. The effects of individual particles are not included in the two-fluid models.

Figure 1 (right) presents the results at $t = 85\Omega_0^{-1}$, which is $65\Omega_0^{-1}$ after the reconnection takes place, when a quasi-steady reconnection layer has formed in the entire dayside magnetopause boundary layer. The transient bulges of the magnetic field have convected tailward out of the domain. The magnetopause has moved closer to the Earth because of the corresponding magnetic flux removal. A large-amplitude rotational discontinuity, RD1, has formed in the entire dayside magnetopause, which is associated with the sharp kinks in the field lines across the boundary layer and a flow acceleration by the field tension force. The negative and positive B_y perturbations are seen in RD1 in the northern and southern hemispheres, respectively. In previous 1-D hybrid simulations by *Lin and Lee* [1994a] an intermediate shock is found to exist in the reconnection layer in the cases with $B_y = 0$ in the magnetosheath and the magnetosphere. In the present simulation the

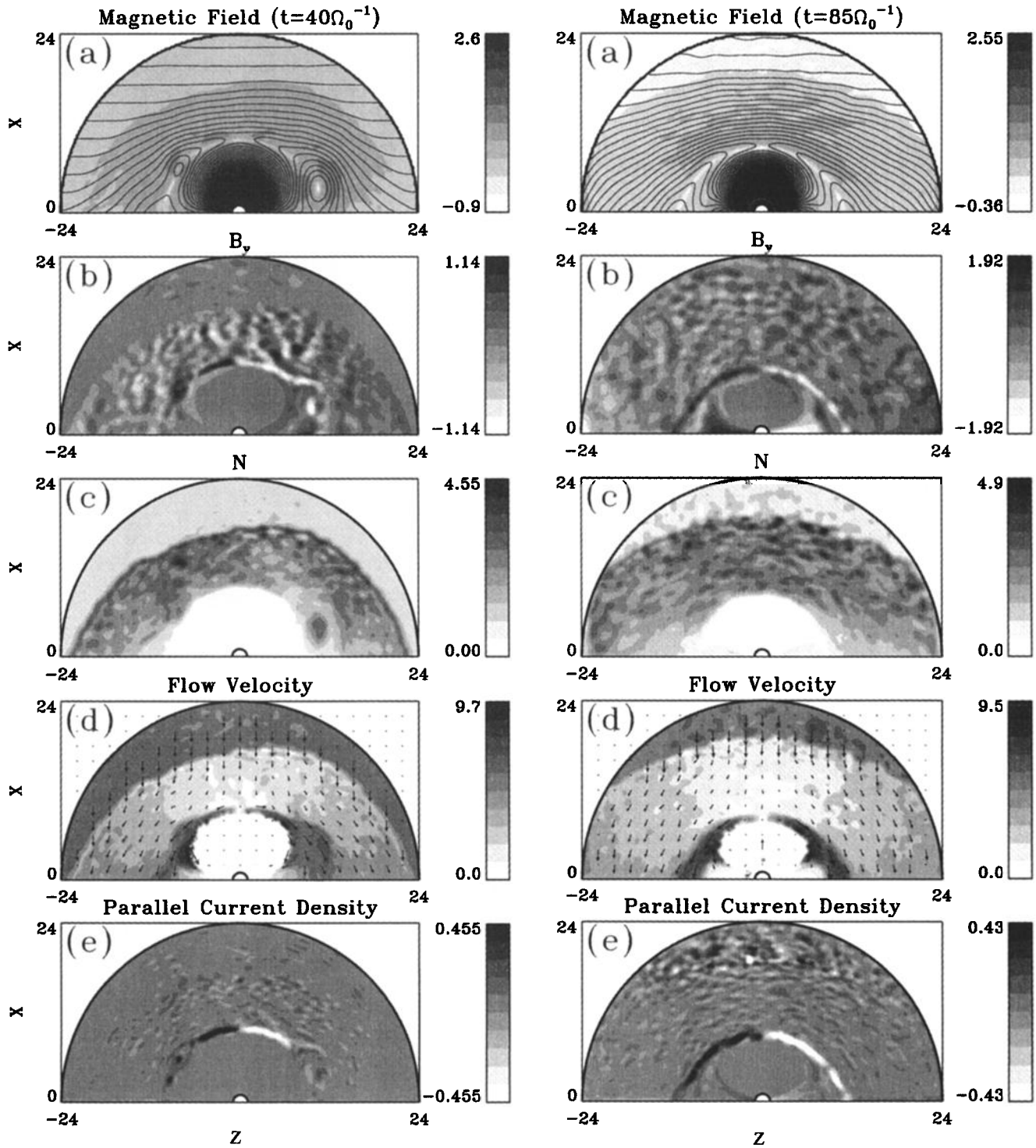

Figure 1. Simulation results of case 1, with $B_{y0} = 0$, at (left) $t = 40\Omega_0^{-1}$ and (right) $t = 85\Omega_0^{-1}$ (right). The positive x points to the Sun, and $+z$ points to the north. (a) Magnetic field lines in the xz plane and gray scale contours of the field magnitude B in the logarithm scale. (b) Contours of B_y. (c) Contours of ion particle number density N. (d) Ion flow vectors and contours of the ion flow speed in the xz plane. (e) Contours of the field-aligned current density $J_{\parallel}$.

spatial resolution is not high enough to distinguish the quite similar kinetic structures of intermediate shock and rotational discontinuity. The magnetic structure of the rotational discontinuity can be seen in the magnetic field hodograms shown below. The front of RD1 extends toward the tail side out of the domain and is expected to bound the plasma mantle.

As to be described later in this section, the structure of RD1 can be identified at distances far enough from the X line. At these distances the B_y component

first grows to a large amplitude as RD1 forms and then oscillates around the finite amplitude. A near circular polarization in the tangential (B_y and B_θ) magnetic field in RD1 occurs at a frequency of 0.2-1Ω_s, where Ω_s is the ion gyrofrequency near the magnetopause. A maximum coherence of 0.7-0.8 between B_y and B_θ also occurs at the oscillation around these frequencies. For the reconnection layer outside the diffusion region the resistive term in the electric field equation (2) can be ignored. From the Faraday's law, the time variation in B_y with a wave frequency near Ω_s is found to be mainly balanced by the θ-derivative of the first-order electric field $\delta E_r \simeq (-V_{i\theta}\delta B_y + B_\theta \delta V_{iy})$. In addition, the discontinuity RD1 is found to slowly oscillate in the Earth frame with a frequency of $\sim 0.01\Omega_s \sim 0.04\Omega_0$. The maximum power of the magnetic field perturbation also occurs at this frequency. Considering that the global spatial scale is $\sim$10 R_E and the convection speed is approximately the magnetopause Alfvén speed V_{As}, this oscillation frequency is nearly the frequency associated with the global convection.

The negative (positive) B_y is also seen in the northern (southern) cusp region. Corresponding to the B_y structures, field-aligned currents with $J_\parallel < 0$ ($J_\parallel > 0$) are seen in the northern (southern) current layer and cusp. Note that $J_\parallel$ in the magnetopause RD1 are nearly the total currents in it. By tracing their paths the Alfvén wave-like perturbations and the associated field-aligned currents in the low altitudes are found to originate from the magnetopause rotational discontinuities during reconnection. At ionospheric altitudes, $J_\parallel$ is, of course, much stronger due to mapping effects. Enhanced ion precipitation also appears in the cusp magnetosphere, as seen in the density contours and the ion flow plot. The actual maximum $J_\parallel$ in the domain is $\sim 0.8J_0$, and the minimum is $\sim -0.7J_0$, both of which are located in the magnetopause current layer. For $B \simeq 10$ nT and $n \simeq 5$ cm^{-3} in the solar wind the normalization scale for $J_0 \simeq 5 \times 10^{-7}$Am^{-2}. Near cusp ionospheric boundaries, $J_\parallel \simeq 0.3J_0$. In the 2-D model the ionospheric current density through the $y\theta$ plane can be mapped to the inner boundary of the magnetopause by a factor of $\sqrt{B_M/B_I} \simeq \sqrt{(1\ R_E)^2/(10\ R_E)^2} = 0.1$, where B_M and B_I are the magnetic field strengths at the magnetopause and the ionosphere, respectively. This factor corresponds to a current density of $0.03J_0$ from the magnetopause. Therefore, for $J_\parallel \simeq 0.5$-$0.8J_0$ in the magnetopause, nearly 4-6% of the magnetopause currents has propagated into the ionosphere. In the 3-D magnetosphere the B field and the cross-section area of flux tubes vary as r^{-3}. This percentage of the magnetopause parallel currents would generate a current density of $J_\parallel \sim 10^{-6}$ Am^{-2} in the ionosphere.

Lee et al. [1985] and *Lin and Lee* [1994c] suggested that leakage of the $J_\parallel$ from the magnetopause rotational discontinuities may contribute to the generation of the traditional cusp/mantle field-aligned current system. The propagation of $J_\parallel$ from the magnetopause to the cusps is indeed found in our simulation. The magnetopause rotational discontinuity is generated by perturbations at the X line. This perturbation convects with the accelerated flows away from the X line, resulting in the RD1 front along the magnetopause. The normal of the RD1 front is largely oblique to the magnetic field. As the discontinuity propagates to higher latitudes, the normal component of the magnetic field becomes larger. The structure of RD1 is thus modified. Some transient Alfvén waves are released from the transition layer, propagating along the field lines. The transient waves in the magnetosphere propagate quickly into the cusp because of the large Alfvén speed in the dipole field region, carrying $J_\parallel$ into the cusp ionosphere. The released waves are stronger toward the north and south poles as the normal component of the magnetic field at RD1 becomes larger, which can be best seen from the B_y contours near the cusp regions. Note that the simulations presented in this paper are not long enough to show the effects of wave reflection from the ionosphere. The $J_\parallel$ flow from the magnetopause to the ionosphere can also be carried by Alfvén waves from transient reconnections at the magnetopause. The upward $J_\parallel$ near the ionosphere in both hemispheres in Figure 1 (right) may contribute to the acceleration of auroral electrons.

In addition to RD1 a layer of small positive (negative) B_y is seen on the earthward side of the northern (southern) magnetopause boundary layer, corresponding to the Hall currents generated by the magnetospheric particles. This layer is associated with a weak Alfvén wave pulse, or in general a weak rotational discontinuity RD2 [*Lin and Lee*, 1994a], which propagates into the magnetosphere, whereas RD1 propagates on the magnetosheath side. This additional structure exists at the inner edge of the magnetopause boundary where the ion density has dropped significantly. It should be noted that at this final time the ion particle density in the magnetosphere has become much lower than the initial value because no effort is made to resupply the ions from the magnetosphere after they are lost into the open boundary layer. Therefore the strength of the simulated RD2 is very weak. The associated field-aligned currents cannot be clearly identified. In this paper, we only identify the currents associated with RD1, whereas $J_\parallel$ in RD2 can propagate directly into the cusp ionosphere.

Figure 2 shows, from the top, hodograms of the magnetic field in the (B_y, B_θ) plane and spatial profiles of B_y (solid curves), B_θ (dotted curves), ion flow velocities V_{iy} (dotted) and $V_{i\theta}$ (solid), magnetic field strength B (solid), and ion density N (dotted) at the final time $t = 85\Omega_0^{-1}$. The θ component of $\mathbf{B}$ and $\mathbf{V_i}$ are nearly along the magnetopause. Shown in Figure 2 from left to right are the cross sections in the quasi-steady reconnection layer along the r coordinate lines from $\theta = 20°$ (near the north pole) to $\theta = 160°$ (south), each for $r = 6\ R_E$ to 24 R_E. Near the X line at $\theta = 90°$ (subsolar region), as shown in the middle column, the B_y

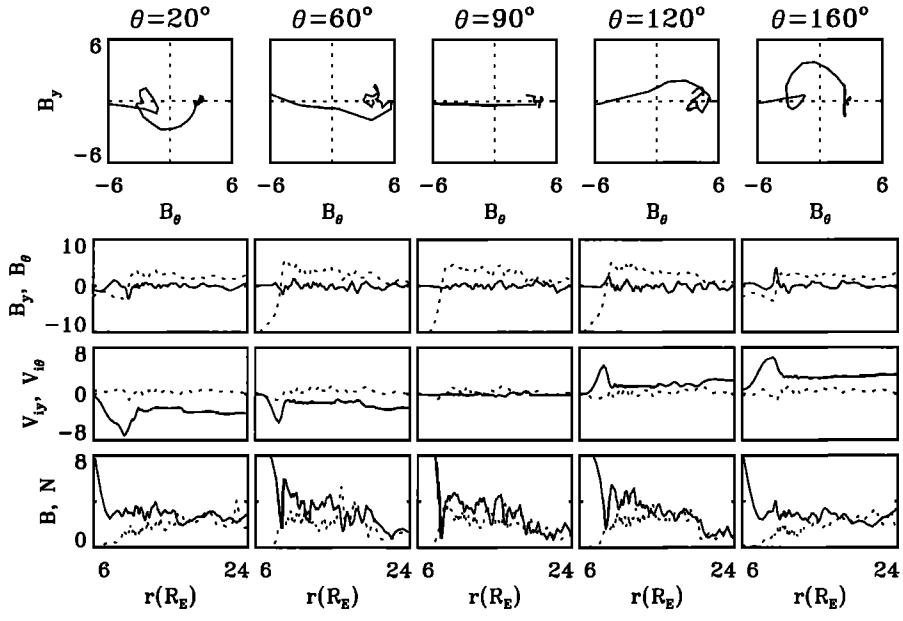

Figure 2. From the top, hodograms of the magnetic field in the (B_y, B_θ) plane and spatial profiles of B_y (solid curves), B_θ (dotted curves), ion flow velocities V_{iy} (dotted) and $V_{i\theta}$ (solid), magnetic field strength B (solid), and ion density N (dotted) along radial lines at $t = 85\Omega_0^{-1}$ in case 1. From left to right are the results at $\theta = 20°$ and 60° (in northern hemisphere), $\theta = 90°$ (sun-Earth line), and $\theta = 120°$ and 160° (southern hemisphere), each for $r = 7\ R_E$ to 24 R_E. All quantities are in normalization units.

component is nearly zero in the magnetopause boundary layer ($r \sim 10\ R_E$). There is no flow acceleration at the X line, as shown in the velocity profiles. In-phase (fast mode) correlations between the fluctuations in B and N are present near the bow shock transition ($r \sim 18\ R_E$), whereas antiphase corrections are seen in the middle of the magnetosheath.

At $\theta = 60°$ and 120° away from the X line, the finite guide field B_y described above develops in the magnetopause rotational discontinuity RD1, across which B_θ changes direction. At both locations an electron sense, or right-hand (with thumb pointing along the normal component of the magnetic field) polarization from the upstream (magnetosheath; $B_\theta > 0$) to the downstream (magnetosphere; $B_\theta < 0$) of RD1 appears in the magnetic field hodograms. Since the normal component of the magnetic field, which is nearly B_r, is negative northward of the X line and positive southward of the X line, the field rotation looks reversed in the B_yB_θ plane at $\theta = 60°$ and 120°. As mentioned earlier, such right-hand field rotation in the magnetopause rotational discontinuity is consistent with the prediction by *Sonnerup* [1979]. The same polarization sense has also been found to dominate the magnetic structure in the flux transfer events at the magnetopause in the 2-D and 3-D hybrid simulations by *Karimabadi et al.* [1999]. Also seen in the second and the fourth column of Figure 2 is that the acceleration in the ion flow starts to appear in the directions away from the X line, with $V_\theta < 0$ at $\theta = 60°$ and $V_\theta > 0$ at $\theta = 120°$. The flow is accelerated from the magnetosheath side through RD1 to a speed of $\sim 4V_{A0}$ at the center of the reconnection layer, while the change of the flow speed from the magnetospheric side is mainly through a modified slow mode wave [*Lin and Lee*, 1994a]. An increase in the parallel temperature $T_\parallel$ (not shown) is also found in the magnetopause. The enhancement in the tangential flow speed $|V_\theta|$ in the magnetopause boundary layer is getting stronger as θ decreases (increases) in the northern (southern) hemisphere.

The structure of the large-amplitude RD1 develops with distance from the X line. At $\theta = 20°$ and 160° the right-hand polarization in the magnetic field becomes nearly circular through RD1, as seen in the field hodograms. A positive (negative) correlation between B_y and V_y is seen in RD1 in the northern (southern) hemisphere, as to be seen below in the Walén relation (9). Note that in the real magnetopause the physical scale lengths, such as the ion inertial length and the ion gyroradius, are smaller than those used in the simulation, so that the full development of the structure of RD1 would appear at a shorter distance from the X line.

For an ideal MHD rotational discontinuity at the magnetopause the density of field-aligned currents in the discontinuity can be written as

$$J_\parallel(r) = \mathbf{J} \cdot \mathbf{B}/B = -(B_t^2/\mu_0 B)d\Phi/dr, \qquad (7)$$

where B_t is the magnitude of the tangential magnetic field in the rotational discontinuity, and the phase angle of the tangential magnetic field $\Phi = \text{atan}(B_y/B_\theta)$. Therefore the sign of $d\Phi/dr$ determines the sign of $J_\parallel$,

with $J_{\|} > 0$ for $d\Phi/dr < 0$ and $J_{\|} < 0$ for $d\Phi/dr > 0$. Our simulation shows that the right-hand rotations with $d\Phi/dr > 0$ and $d\Phi/dr < 0$ are generated in the northern and southern hemispheres, respectively. Correspondingly, upward field-aligned currents with $J_{\|} < 0$ ($J_{\|} > 0$) can leak into the ionosphere in both hemispheres.

Another feature to be noticed is that while the magnetosheath flow gradually becomes significant as θ increases, there is a general trend that the magnetopause boundary layer is getting thicker. This is partly due to the shear flow effects, which reduces the magnetic tension force and thus the strength of RD1 [*Lin and Lee*, 1994b]. However, the variation in the strength of RD1 is also due to the variations in the geometry of the magnetic field lines and the external pressure from the solar wind.

According to the MHD Rankine-Hugoniot (RH) jump conditions [*Landau and Lifshitz*, 1960] the Walén relation has to be satisfied across a rotational discontinuity. In a plasma with a temperature anisotropy this relation states that

$$\Delta \mathbf{V_t} = \pm \Delta \mathbf{V'_{At}}, \tag{8}$$

where $\Delta \mathbf{V_t}$ is the the change of the tangential flow velocity across the rotational discontinuity, the plus (minus) sign is applied to rotational discontinuities with a normal component of the upstream inflow velocity parallel (antiparallel) to the normal component of the magnetic field, $\Delta \mathbf{V'_{At}}$ is the corresponding change in the Alfvén velocity $\mathbf{V'_{At}}$, $\mathbf{V'_{At}} = \mathbf{V_{At}}[1 - (\beta_{\|} - \beta_{\perp})/2]^{1/2}$, $\mathbf{V_{At}}$ is the tangential Alfvén velocity in the ideal MHD, and $\beta_{\|}$ and $\beta_{\perp}$ are the plasma beta values associated with the parallel and perpendicular pressures, respectively. On the other hand, most of the satellite observations at the magnetopause based on ion velocities showed that

$$\Delta \mathbf{V_{it}} = \pm A_i \Delta \mathbf{V'_{At}}, \tag{9}$$

where $A_i \simeq 0.7$-0.9 is the average ion Walén ratio [*Papamastorakis et al.*, 1989; *Sonnerup et al.*, 1981]. When considering the ion finite Larmor radius effects, it is the electron fluid that is "frozen in" the magnetic field, as shown in (2). *Scudder et al.* [1999] examined the Walén relation based on the change in the electron flow velocity, $\Delta \mathbf{V_e}$, across the rotational discontinuities at the magnetopause and found that the electron Walén relation is very well satisfied. Nevertheless, the electron flow velocity $\mathbf{V_e}$ cannot simply represent the plasma velocity in the MHD. The difference between $\mathbf{V_i}$ and $\mathbf{V_e}$ is equivalent to the currents in the rotational discontinuity. The direction of the currents, which is related to the sense of the magnetic field polarization, can imply either $V_{it} > V_{et}$ or $V_{it} < V_{et}$. The modification of the Walén relation in rotational discontinuities and Alfvén waves were further examined by *Wu and Lee* [2000] using the Hall-MHD formulation. They found that the dispersive structure of the ion density in the rotational discontinuity results in the deviation of $\Delta \mathbf{V_{it}}$ from $\Delta \mathbf{V_{At}}$. The product of the ion and electron Walén ratios $A_i A_e = 1$, where $A_e = V_{et}/V_{At}$, and $A_i < 1$ ($A_i > 1$) in the transition layer of the rotational discontinuities with a right-hand (left-hand) polarization.

Figure 3 (left) shows the variations of the tangential components of the ion and electron flow velocities, $\Delta \mathbf{V_{it}}$ and $\Delta \mathbf{V_{et}}$, through RD1 around $\theta = 60°$ as a function of the variation in the corresponding Alfvén velocity, $\Delta \mathbf{V'_{At}}$, in case 1. The pluses show the variations of the θ component velocities versus the variations in $V'_{A\theta}$, and the dots show the corresponding variations in the y components. All quantities are normalized to the Alfvén speed V_{A0} in the solar wind. The variation in the velocities is measured as the difference between the velocities at various locations (r, θ) in RD1 and the velocity at a location (r_u, θ), where r_u is a radial distance just upstream of RD1. The solid diagonal line in each plot represents $\Delta \mathbf{V_{it,et}} = \Delta \mathbf{V_{At}}'$. Note that in the northern hemisphere ($\theta < 90°$) the normal inflow velocity (from the magnetosheath to the magnetosphere) is parallel to the normal magnetic field component (roughly $\mathbf{B_r}$) at the magnetopause, and thus the pluses should be taken in the right-hand side of (9). At $\theta = 60°$ the Walén ratio $A_i \simeq 0.77 \pm 0.12$ based on a least

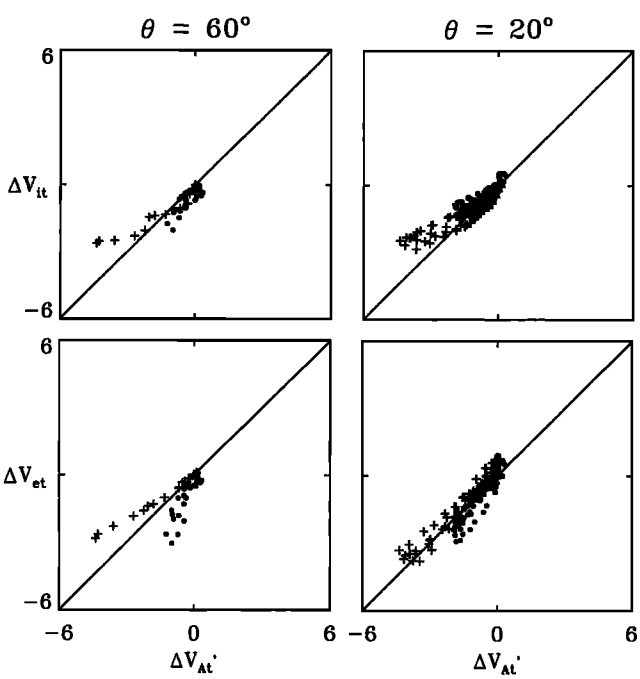

Figure 3. Variations of the tangential components of ion flow velocities, $\Delta V_{i\theta}$ (pluses) and ΔV_{iy} (dots), and variations of electron flow velocities, $\Delta V_{e\theta}$ (pluses) and ΔV_{ey} (dots), throughout RD1 around (left) $\theta = 60°$ and (right) $\theta = 20°$ as a function of the corresponding $\Delta V'_{A\theta}$ and $\Delta V'_{Ay}$, where $\mathbf{V'_A}$ is the Alfvén velocity modified by the temperature anisotropy. All quantities are normalized to the Alfvén speed V_{A0} in the solar wind, and the velocity variations along each θ line are relative to the corresponding values just upstream of RD1. The solid diagonal lines represents $\Delta \mathbf{V_{i,e}} = \Delta \mathbf{V_A}'$.

squares fit for all the data points in Figure 3 (top left). The corresponding standard deviation in ΔV_{it}, which also includes the short-wavelength numerical fluctuations due to the finite number of particles per cell, is nearly ± 0.50. The Walén ratio $A_e \simeq 0.81 \pm 0.16$, with a standard deviation in ΔV_{et} nearly equal to ± 0.81. The θ and y components, however, have quite different Walén ratios for both ion and electron velocities. The negative ion and electron flow velocities in RD1 are attributed to the Alfvén mode. However, since the B_y component in RD1 has not well developed to the large amplitude yet at $\theta = 60°$, the ion Walén ratio is larger than that of the θ component. The changes in the y component electron velocities are even larger than those in the y component ion velocities because of the positive J_y in the magnetopause, and thus the electron Walén ratio for the y component is quite large. The average ion Walén ratio ~ 0.70 for the θ component alone and ~ 1.4 for the y component alone, whereas the average electron Walén ratios are ~ 0.70 and 2.2 for the θ and y components, respectively.

Figure 3 (right) shows the results at $\theta = 20°$ farther away from the X line. The results of the ion and electron flow velocities are very similar at this distance. The Walén relation is well satisfied for the tangential components of electron velocities, with an overall $A_e \simeq 0.99 \pm 0.07$. The corresponding standard deviation of ΔV_{et} is about ± 0.45. In the ion Walén fit plots shown in Figure 3 (top right), as $|\Delta V'_{A\theta}|$ and $|\Delta V'_{Ay}|$ increase from zero, the slope A_i first appears very close to 1, but then $|\Delta \mathbf{V_i}|$ becomes smaller than required by the MHD Walén relation. The overall ion Walén ratio $A_i \simeq 0.71 \pm 0.06$. In the Hall-MHD formulation by *Wu and Lee* [2000] the Walén ratios $A_i(r) < 1$ and $A_e(r) > 1$ for the right-hand polarized rotational discontinuity. Note that although the slope $A_i(r) < 1$ in the transition of a rotational discontinuity with the right-hand field polarization, the values A_i and A_e should be equal to 1 if one only measures the difference between the nonzero components of the upstream and the downstream velocities, since the dispersive structure due to the Hall effects only modifies the internal transition of RD1. The 1-D hybrid simulations by *Lin and Lee* [1994a] have found that the RH jump conditions are well satisfied in rotational discontinuities at the magnetopause. In the present 2-D simulation the jump in the tangential component $V_{i\theta}$ across RD1 from upstream to downstream is obviously less than the jump in the corresponding Alfvén velocity. Throughout RD1, the ion $A_i(r) < 1$, and the electron $A_e(r) \simeq 1$. This general trend that the Walén ratios A_i and A_e in the transition of the 2-D RD1 are smaller than those obtained from the 1-D models is consistent with the previous hybrid simulation by *Lin and Xie* [1997]. Their simulation shows that at the distances from the X line where the rotational discontinuity or intermediate shock is not well separated from other waves in the reconnection layer, the Walén relation cannot be satisfied, and the plasma flow is not accelerated to that predicted by the jump conditions of rotational discontinuity. This effect may reduce A_i and A_e, leading to $A_e(r)$ in the RD1 transition very close to 1, as seen from Figure 3 (bottom right). It should be noted, as mentioned earlier, that the spatial resolution in the present global simulation is not high enough for the real magnetopause structure because the ion inertial lengths are larger than those in reality, and thus the separation between RD1 and other waves as a function of the distance from the X line is slower.

In case 2 the IMF $B_y = 0.4B_0$, while the magnetic field strength and plasma quantities in the solar wind and the magnetosphere are the same as those in case 1. Figure 4 (left) shows the field line configuration, superposed on the contour plot of the magnetic field strength in the logarithm scale, and the contours of B_y and $J_\parallel$ at $t = 100\Omega_0^{-1}$ in the quasi-steady state of the reconnection. Although $B_y > 0$ in the magnetosheath, the pattern of B_y in the magnetopause boundary layer is similar to that in case 1. In the transition of RD1, B_y has negative fluctuations in the northern hemisphere and positive fluctuations in the southern hemisphere. Correspondingly, $J_\parallel < 0$ and $J_\parallel > 0$ are seen in the northern and southern boundary layers, respectively. As in case 1, some of these currents flow into the cusp ionosphere, producing upward field-aligned currents in both hemispheres. The actual maximum of $J_\parallel$ is $0.9J_0$ and the minimum is $-0.8J_0$, which are again located in the front side magnetopause. The sense of $J_\parallel$ as a function of the IMF B_y will be further discussed in case 5.

Figure 4 (right) presents hodograms of the magnetic field across the magnetopause boundary layer at the symmetric locations of $\theta = 60°$ and $120°$, $\theta = 50°$ and $130°$, $\theta = 40°$ and $140°$, and $\theta = 30°$ and $150°$. Similar to case 1, from $\theta = 120°$ to $150°$, the right-hand rotation in the magnetic field in RD1 develops into a more circular polarization as the distance from the X line increases. Although still right-handed, the patterns in the hodograms of the northern hemisphere with $\theta < 60°$, however, are not quite circular, and the perturbation amplitude in B_y is small. Note that for a right-hand polarization in the northern hemisphere, the magnetic field has to follow a rotation angle of $|\Delta\Phi| > 180°$ from the magnetosheath to the magnetosphere.

In case 3 the IMF $B_{y0} = 0.8B_0$. Similar to case 2, large-amplitude, right-hand circular polarizations are present in the southern hemisphere from $\theta = 120°$ to $150°$. In the northern hemisphere with $\theta < 90°$, however, the right-hand polarization of the magnetic field in RD1 becomes nearly linear at $\theta < 40°$, and the rotation sense starts to reverse at $\theta = 30°$.

We now show a case in which the IMF $B_y < 0$. In case 4 the initial magnetic field and plasma quantities are the same as those in case 3, except the sign of B_{y0} is reversed, i.e., $B_{y0} = -0.4B_0$. Figure 5 (left) shows the contour plots of B_y and $J_\parallel$ in the stage when the

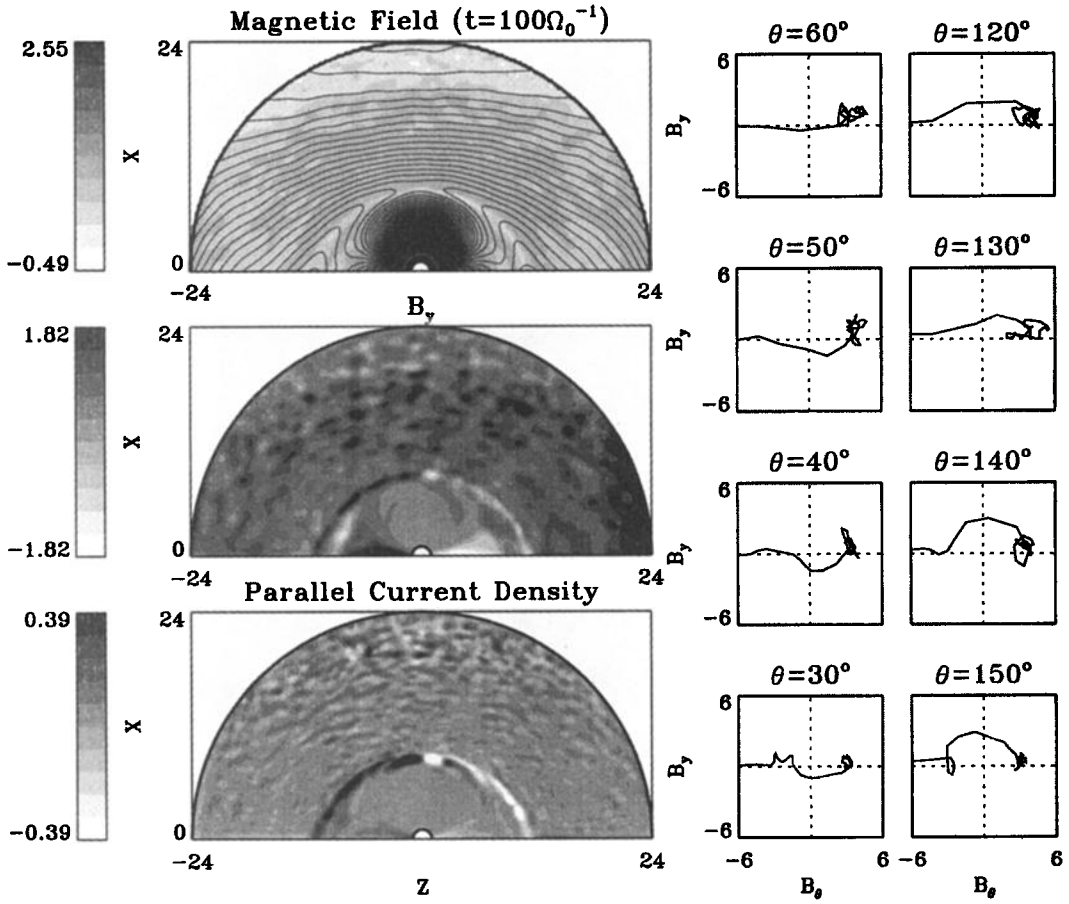

Figure 4. (left) Field line configuration, superposed on the contour plot of B in the logarithm scale, and contours of B_y and $J_\parallel$ at $t = 100\Omega_0^{-1}$ in case 2 with $B_{y0} = 0.4$. (right) Hodograms of the magnetic field across the magnetopause at the symmetric locations of $\theta = 60°$ and 120°, $\theta = 50°$ and 130°, $\theta = 40°$ and 140°, and $\theta = 30°$ and 150°.

quasi-steady reconnection layer has formed in the entire dayside magnetopause boundary. In the reconnection layer the signs of the B_y perturbations in the northern and southern hemispheres are the same as those in case 3, although the sign of the IMF B_y is different from that in case 3. As a result, upward $J_\parallel$ are again seen in the northern and southern cusp regions. The hodograms of the magnetic field at various locations along the magnetopause are shown in Figure 5 (right). Similar to the cases with $B_{y0} > 0$, right-hand polarizations in the magnetic field are present in RD1 at locations with both $\theta < 90°$ and $\theta > 90°$. Nevertheless, with $B_y < 0$ in the magnetosheath, for a right-hand polarization in the southern hemisphere the magnetic field has to go through a rotation angle $|\Delta\Phi| > 180°$, whereas in case 3, $|\Delta\Phi| > 180°$ appears in the northern hemisphere. The evolution of RD1 in the northern and southern hemisphere is opposite to that in case 3. A large-amplitude, nearly circular polarization in the magnetic field gradually develops in the northern hemisphere away from the X line, as shown in the hodogram near $\theta = 40°$ and 30°, whereas the field rotation pattern in the southern hemisphere becomes quite flat as the distance from the X line increases.

It is seen from the above cases that the magnetic field tends to follow a right-hand polarization when the magnetopause rotational discontinuity is formed by the reconnection. This right-hand rotation is stable if the field rotation angle $|\Delta\Phi| < 180°$ across RD1 but not quite stable for $|\Delta\Phi| > 180°$. In previous 1-D hybrid simulations of rotational discontinuity it is found that for a rotational discontinuity initially with $|\Delta\Phi| > 180°$, the discontinuity will evolve to a new structure with $|\Delta\Phi| < 180°$ by the reversal of the field rotation sense or by losing several 360° rotations in the magnetic field. That is, given enough evolution time, the rotational discontinuity converges to a final stable structure in which the field rotation follows the shortest angular path $|\Delta\Phi|$ [*Swift and Lee*, 1983; *Krauss-Varban et al.*, 1995; *Lin and Lee*, 2000]. The transient evolution time increases with the initial width of the rotational discontinuity but decreases with the initial $|\Delta\Phi|$ [*Krauss-Varban et al.*, 1995; *Lin and Lee*, 2000]. In order to see the evolution of the rotational discontinuities in our global 2-D simulation, we have run several cases with a thinner magnetopause.

The initial condition in case 5 is the same as that in case 3, with $B_{y0} = 0.8B_0$, but the ion inertial length is

reduced by a factor of 2 everywhere in the simulation domain. Thus the new ion inertial length is $\sim 0.08\ R_E$ in the solar wind and is $\sim 0.05\ R_E$ in the magnetosheath region adjacent to the magnetopause. The half-width of the initial magnetopause current sheet is also set to a smaller value of $0.05\ R_E \simeq 320$ km. It is found that the halfwidth of the magnetopause rotational discontinuity RD1 is maintained at ~ 0.08-$0.15\ R_E$, which is thinner than that in case 3. Although the thickness of RD1 in units of λ_s is nearly equal to that in case 3, the RD1 front along the magnetopause is longer in terms of λ_s, so the development of RD1 along the magnetopause is faster in units of $R_E s^{-1}$. The hodograms of the magnetic field across the magnetopause boundary layer at the final simulation time are shown in Figure 6. The evolution of the magnetic field in the $\theta > 90°$ region, where the field direction change $|\Delta\Phi| < 180°$, as a function of the distance to the X line is very similar to that in case 3 with a thicker magnetopause current layer. The evolution in the northern hemisphere ($\theta < 90°$), however, is quite different. As θ decreases from 60° to 30°, the original right-hand polarization with $\Delta\Phi \simeq -210°$ in the magnetic field gradually turns to a left-hand rotation, which has the shorter angular path of $\Delta\Phi \simeq 150° < 180°$, as seen from Figure 6 (left). This result is consistent with previous 1-D hybrid simulations of rotational discontinuity. Such evolution as a function of θ is slower for a smaller B_{y0}.

Correspondingly, in this case with IMF $B_{y0} > 0$ the currents $J_\parallel$ injected to the northern cusp ionosphere from the magnetopause are mainly positive, or downward, currents. Although the structure of RD1 in the northern hemisphere still shows a portion of right-hand polarization on the upstream (magnetosheath side) edge, the main large-amplitude rotation becomes left-handed at far distances from the X line. In the southern hemisphere, $J_\parallel$ remains positive and thus is upward. For a similar case with an IMF $B_{y0} < 0$ the sense of $J_\parallel$ in either hemisphere is opposite to that in case 5.

The pluses in Figure 7 show the variations $\Delta V_{i\theta}$ and $\Delta V_{e\theta}$ as a function of $\Delta V'_{A\theta}$ through RD1 along $\theta = 30°$ and 150° obtained from case 5. In the southern hemisphere at $\theta = 150°$ an average ion Walén ratio $A_i \simeq (0.60 \pm 0.07) < 1$ and an electron $A_e \simeq (0.80 \pm 0.05)$ closer to 1 are found in the right-handed RD1, similar to case 1. Note that in the southern hemisphere

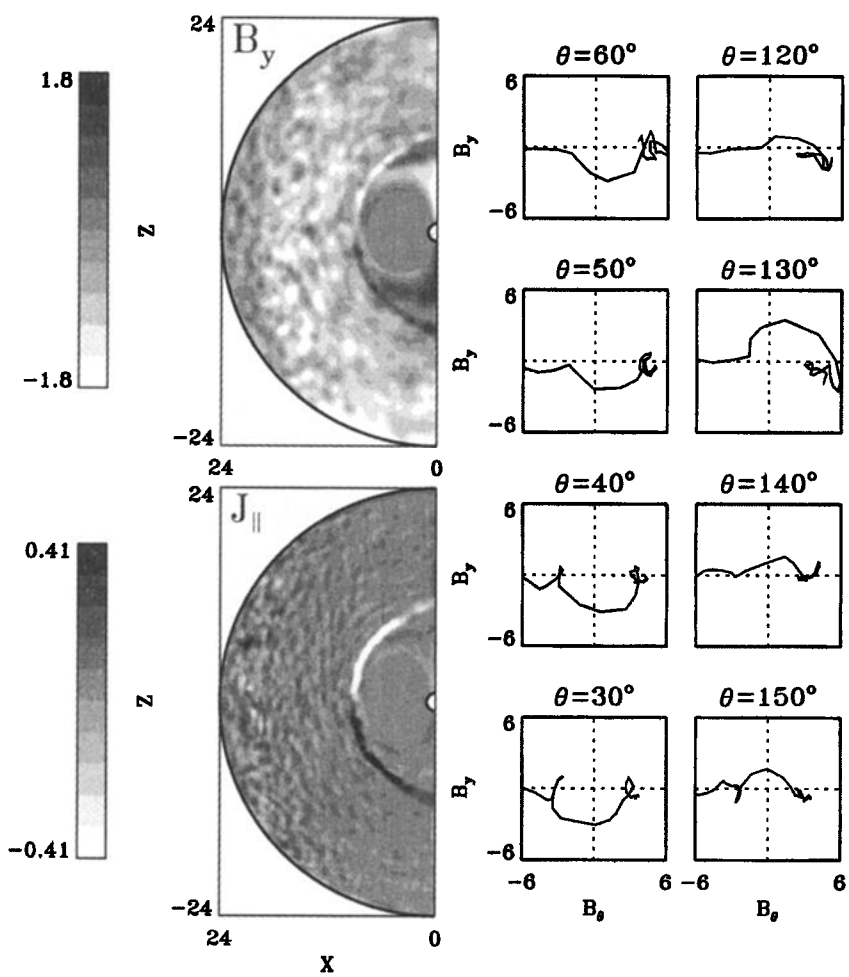

Figure 5. (left) Contour plots of B_y and $J_\parallel$ in case 4 with $B_{y0} = -0.4$. (right) Field hodograms at various locations at the magnetopause.

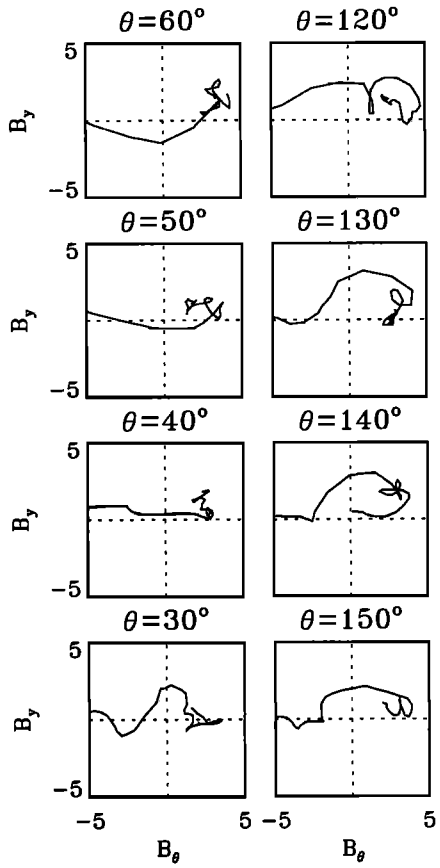

Figure 6. Hodograms of the magnetic field across the magnetopause reconnection layer in case 5 with $B_{y0} = 0.8$ and with a thin magnetopause.

the normal inflow velocity from the magnetosheath is antiparallel to the normal component of the magnetic field, and thus the sign of $\Delta V_{i,e\theta}$ is opposite to that of $\Delta V'_{A\theta}$, as shown in Figure 7 (right). In the northern hemisphere at $\theta = 30°$ the polarization of RD1 has become left-handed (ion sense). A good correlation with an average $A_i \simeq 0.70 \pm 0.08$ and an average $A_e \simeq 0.75 \pm 0.07$ is also obtained in the rotational discontinuity. *Wu and Lee* [2000] showed that in the Hall MHD, a left-hand-polarized rotational discontinuity should possess an $A_e(r) < 1$ and an $A_i(r) > 1$. Our 2-D hybrid simulation shows that similar to case 1, the 2-D effects can reduce the ion and electron Walén ratios. Both A_e and A_i are less than 1 in the left-hand RD1 within the reconnection time of $250\Omega_s^{-1}$. Given that the spatial resolution in our 2-D hybrid particle simulation is not as high as that in 1-D models, some of the detailed dispersive structure of RD1 may not be fully captured.

In case 5 it takes $\sim 180\Omega_s^{-1}$ for the right-hand field rotation in RD1 in the northern hemisphere to reverse its sense. Since the convection speed (in units of $R_E s^{-1}$) in our simulation is larger than that on the real magnetopause, the propagation speed of the rotational discontinuity at the real magnetopause would be much slower than that in the simulation. Thus the propagation distance, from the X line, for a magnetopause rotational discontinuity to reverse the magnetic field polarization would be much shorter. In case 5 the polarization reverses within a θ range of 55°. If scaled down by a factor of 7 to 10, this range would correspond to a distance of $\sim 1\ R_E$ from the diffusion region of reconnection. For a magnetosheath ion density of 1-10 cm^{-3} we obtain an ion inertial length $\lambda_s \sim$ 70-230 km. For most of the observed thin magnetopause rotational discontinuities with a thickness of 100-500 km, corresponding to a few λ_s, the magnetic field should have evolved to a smallest rotation angle of $|\Delta\Phi| < 180°$, as found by *Berchem and Russell* [1982].

On the other hand, for a magnetopause transition layer that is relatively thick, which may be present in 3-D time-dependent reconnections such as FTEs, the magnetic field may follow a large rotation angle. In this case, it is possible that the field-aligned currents generated in the reconnection are dominated by positive currents in the northern hemisphere and negative currents in the southern hemisphere, leading to upward $J_{||}$ in both the northern and southern cusp ionosphere regions. The upward $J_{||}$ may produce an upward electric field, increase the electron precipitation, and drive aurora activity in the ionosphere.

4. Summary

In summary, a 2-D global hybrid particle simulation has been performed for magnetic reconnection at the

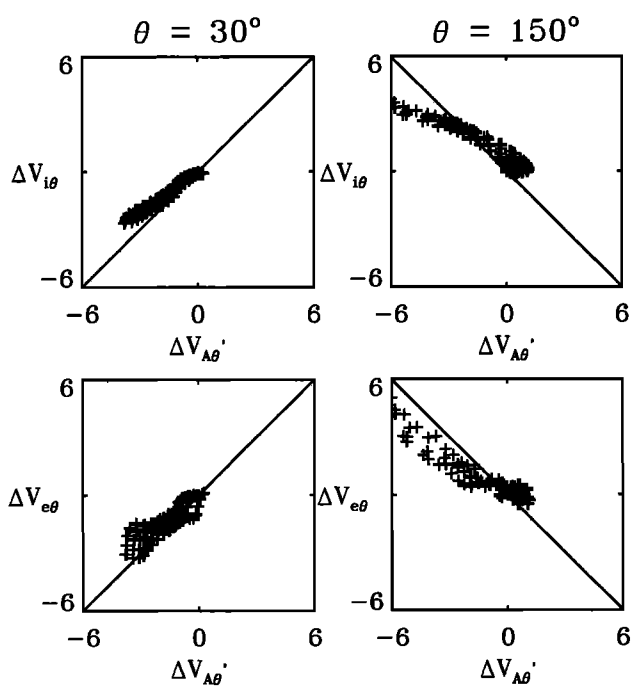

Figure 7. Variations $\Delta V_{i\theta}$ and $\Delta V_{e\theta}$ (pluses) as a function of $\Delta V'_{A\theta}$ through RD1 along $\theta = 30°$ and 150° in case 5.

dayside magnetopause in the noon-midnight meridian plane. The main results are summarized below.

1. A large-amplitude rotational discontinuity RD1 is present in the magnetopause boundary layer due to a single X line reconnection, consistent with previous hybrid simulation near the X line. RD1 carries the main electric current in the magnetopause, and the thickness of RD1 is of the order of the local ion inertial length. Associated with the field line kinks in RD1, accelerated flows are present in the magnetopause boundary layer. A weak rotational discontinuity RD2 is also seen on the magnetospheric side of the magnetopause reconnection layer, which carries a small amplitude magnetic field perturbation.

2. Strong field-aligned currents are present in RD1 due to the rotation of the tangential magnetic field in the (B_y, B_θ) plane. As RD1 first forms after reconnection, the tangential magnetic field follows a right-hand (electron sense) polarization in both the northern and southern hemispheres, leading to $B_y < 0$ in RD1 in the northern magnetopause and $B_y < 0$ in the southern hemisphere. This polarization is consistent with the theoretical predictions of *Sonnerup* [1979]. Correspondingly, field-aligned currents with $J_\parallel < 0$ are generated in the northern hemisphere and $J_\parallel > 0$ are generated in the southern hemisphere.

In 1-D and 2-D MHD simulations [*Lin and Lee*, 1994a, 1994c, 1999] the magnetic field variation always follows a short angular path of $|\Delta\Phi| \leq 180°$ in a rotational discontinuity generated in magnetic reconnection. Therefore the associated field-aligned currents always have $J_\parallel > 0$ for a magnetosheath $B_y > 0$ and $J_\parallel < 0$ for a magnetosheath $B_y < 0$, whether in the northern or southern hemisphere. Similar polarities of $J_\parallel$ has also been found by *Ma and Lee* [1999] from a 3-D MHD simulation of magnetic reconnection. In our hybrid simulation, however, the magnetic field prefers a right-hand rotation due to the Hall effects when the rotational discontinuity just forms, regardless of the magnitude of $|\Delta\Phi|$ or the sign of B_y in the magnetosheath.

3. As RD1 propagates away from the X line, if the right-handed rotation $|\Delta\Phi|$ exceeds 180°, the tangential magnetic field tends to evolve to a more stable left-hand structure with a smaller field rotation angle $|\Delta\Phi| < 180°$, similar to the MHD results. This evolution proceeds more quickly for a thinner magnetopause and a larger ratio $|B_y/B_z|$. Note that the for a given IMF B_{y0} the ratio $|B_y/B_z|$ in the 2-D simulation is smaller than in the real 3-D cases owing to the pile up of the latitudinal magnetic flux in front of the magnetopause. On the basis of the physical parameters at the magnetopause, it is expected that most of the observed thin magnetopause rotational discontinuities possess a magnetic field rotation of $|\Delta\Phi| < 180°$. Therefore associated with a thin rotational discontinuity at the magnetopause in either hemisphere, $J_\parallel > 0$ should be generated for an IMF $B_{y0} > 0$ and $J_\parallel < 0$ should exist for an IMF $B_{y0} < 0$. Note that the 3-D MHD simulation by *Ma and Lee* [1999] showed that for a reconnection with a short X line (in y), field-aligned currents with opposite signs can be distributed along y.

4. The Walén relation is examined for both the electron and the ion flows in the magnetopause rotational discontinuity. For a right-hand RD1 the ion Walén ratio $A_i < 1$, and the electron A_e can be ~1. For a left-hand RD1, both A_i and A_e are less than unity. However, in general, the Walén relation can be nearly satisfied for both ions and electrons. While the Hall-MHD formulation predicts that $A_i < 1$ and $A_e > 1$ for a right-hand rotational discontinuity and $A_i > 1$ and $A_e < 1$ for a left-hand rotational discontinuity, our results show A_i and A_e in the RD1 transition are, in general, less than those obtained from the Hall-MHD simulation. Note that the presence of finite electron pressures in the rotational discontinuities is not considered in this simulation. While our simulation shows that the jump conditions of rotational discontinuity are nearly satisfied in RD1 at an enough distance from the X line, the structure of the rotational discontinuities may be modified by smaller-scale electron dynamics.

5. The structure of the thin magnetopause rotational discontinuity changes in the high latitude regions in response to the changing geometry of the field lines. Some transient Alfvén mode waves carrying part (~5%) of the magnetopause $J_\parallel$ propagate along the field lines from the magnetopause to the cusp ionosphere, while the majority of the $J_\parallel$ of RD1 remain as magnetopause currents. Therefore, for IMF $B_{y0} > 0$, downward $J_\parallel$ is generated in the northern hemisphere and upward $J_\parallel$ in the southern hemisphere, whereas for IMF $B_{y0} < 0$ the sense of $J_\parallel$ reverses in both hemispheres. This result is consistent with the predictions of previous MHD simulations.

6. In the cases in which the magnetopause rotational discontinuities or Alfvén waves have not evolved to the stable magnetic polarization, which can occur following transient reconnection with a short reconnection time or in a quasi-steady magnetopause current layer thicker than several ion inertial lengths, our hybrid simulation suggests that upward field-aligned currents ($J_\parallel < 0$ in the northern hemisphere and $J_\parallel > 0$ in the southern hemisphere) associated with a right-hand magnetic field rotation may propagate into the cusp ionosphere in both hemispheres, regardless of the sign of the IMF B_{y0}. Since the upward $J_\parallel$ may accelerate the precipitating electrons in the ionosphere, this result, which is due to the Hall effects and cannot be obtained from MHD simulations, can provide a mechanism for the generation of the dayside transient auroral forms by time-dependent reconnection [e.g., *Fasel et al*, 1993].

7. The magnetosheath ions penetrate through the magnetopause rotational discontinuity into the magnetopause boundary layer. Strong ion injections are seen in the cusp magnetosphere.

Finally, it should be noted that for the cases shown in this paper the simulation run was terminated when the

magnetopause currents reach the ionospheric boundary. In the simulation, there is no returning magnetic fluxes from the nightside as in the real global magnetosphere, and thus the magnetopause will erode continuously if the simulation proceeds. The effects of the ionospheric conductivity on the magnetopause currents are not studied in this simulation. Observations [e.g., *Ohtani et al.*, 2000] suggest that the ionospheric conductivity determines the intensity of field-aligned currents and may even affect the way the magnetosphere interacts with the solar wind. The closure of the global current system of the magnetosphere and the global convection patterns under various IMF B_y cannot be studied by this 2-D model. In addition, the strength of the $J_{\|}$ flowing into the cusp ionosphere as a function of the IMF B_y are also not investigated in detail. In the real 3-D magnetosphere the strength of the low altitude $J_{\|}$ that comes from the magnetopause may be stronger than that obtained in the 2-D model because the magnetic field strength and thus the cross section areas of magnetic flux tubes vary as r^{-3} in the 3-D dipole field, whereas B varies as r^{-2} in the 2-D dipole field.

Acknowledgments. This work was supported by NASA grant NAG5-8081 and NSF grant ATM-9805550 to Auburn University. Computer resources were provided by the National Partnership for Advanced Computational Infrastructure and the Alabama Supercomputer Center.

Janet G. Luhmann thanks Vincent A. Thomas and another referee for their assistance in evaluating this paper.

References

Berchem, J., and C. T. Russell, Magnetic field rotation through the magnetopause: ISEE 1 and 2 observations, *J. Geophys. Res.*, *87*, 8139, 1982.

Dungey, J. W., Interplanetary magnetic field and the auroral zones, *Phys. Rev. Lett.*, *6*, 47, 1961.

Fasel, G. J., L. C. Lee, and R. W. Smith, A mechanism for the multiple brightenings of dayside poleward-moving forms, *Geophys. Res. Lett.*, *20*, 2247, 1993.

Fedder, J. A., and J. G. Lyon, The solar wind-magnetosphere-ionosphere current-voltage relationship, *Geophys. Res. Lett.*, *14*, 880, 1987.

Fuselier, S. A., K. J. Trattner, S. M. Petrinec, C. T. Russell, and G. Le, Cusp observations of high- and low-latitude reconnection for northward interplanetary magnetic field, *J. Geophys. Res.*, *105*, 253, 2000.

Gosling, J. T., M. F. Thomsen, S. J. Bame, and C. T. Russell, Accelerated plasma flows at the near-tail magnetopause, *J. Geophys. Res.*, *91*, 3029, 1986.

Gosling, J. T., M. F. Thomsen, S. J. Bame, R. C. Elphic, and C. T. Russell, Observations of reconnection of interplanetary and lobe magnetic field lines at the high-latitude magnetopause, *J. Geophys. Res.*, *96*, 14,097, 1991.

Heyn, M. F., et al., The structure of reconnection layer, *J. Plasma Phys.*, *40*, 235, 1988.

Karimabadi, H., D. Krauss-Varban, N. Omidi, and H. X. Vu, Magnetic structure of the reconnection layer and core field generation in plasmoids, *J. Geophys. Res.*, *104*, 12,313, 1999.

Kessel, R. L., S. J. Chen, J. L. Green, S. F. Fung, S. A. Boardsen, L. C. Tan, T. E. Eastman, J. D. Craven, and L. A. Frank, Evidence of high-latitude reconnection during northward IMF: Hawkeye observations, *Geophys. Res. Lett.*, *23*, 583, 1996.

Krauss-Varban, D., H. Karimabadi, and N. Omidi, Kinetic structure of rotational discontinuities: Implications for the magnetopause, *J. Geophys. Res.*, *100*, 11,981, 1995.

Krauss-Varban, D., H.. Karimabadi, and N. Omidi, Two-dimensional structure of the co-planar and non-coplanar magnetopause during reconnection, *Geophys. Res. Lett.*, *26*, 1235, 1999.

Landau, L. D., and E. M. Lifshitz, *Electrodynamics of Continuous Media*, Pergamon New York, 1960.

Lee, L. C., J. R. Kan, and S.-I. Akasofu, On the origin of the cusp field-aligned currents, *J. Geophys.*, *57*, 217, 1985.

Lee, L. C., L. Huang, and J. K. Chao, On the stability of rotational discontinuities and intermediate shocks, *J. Geophys. Res.*, *94*, 8813, 1989.

Levy, R. H., H. E. Petschek and G. L. Siscoe, Aerodynamic aspects of magnetospheric flow, *AIAA J.*, *2*, 2065, 1964.

Lin, Y., and L. C. Lee, Structure of reconnection layers in the magnetosphere, *Space Sci. Rev.*, *65*, 59, 1994a.

Lin, Y., and L. C. Lee, Reconnection layer at the flank magnetopause in the presence of shear flow, *Geophys. Res. Lett.*, *21*, 855, 1994b.

Lin, Y., and L. C. Lee, Generation of region 1 and mantle field-aligned currents by the secondary rotational discontinuity, in *Solar Wind Sources of Magnetospheric Ultra-Low-Frequency Waves, Geophys. Monogr. Ser.*, vol. 81, edited by M. Engebreton, K. Takahashi, and M. Scholer, pp. 213-221, AGU, Washington, D. C., 1994c.

Lin, Y., and L. C. Lee, Reconnection layers in two-dimensional magnetohydrodynamics and comparison with one-dimensional Riemann problem, *Phys Plasmas*, *6*, 3131, 1999.

Lin, Y., and L. C. Lee, Magnetic field rotation and the transition width in rotational discontinuities and Alfvén wave trains, *J. Geophys. Res.*, *105*, 139, 2000.

Lin, Y., and H. Xie, Formation of reconnection layer at the dayside magnetopause, *Geophys. Res. Lett.*, *24*, 3145, 1997.

Lyu, L. H., and J. R. Kan, Nonlinear two-fluid hydromagnetic waves in the solar wind: Rotational discontinuity, soliton, and finite-extent Alfvén wave train solutions, *J. Geophys. Res.*, *94*, 6523, 1989.

Ma, Z. W., and L. C. Lee, A simulation study of generation of field-aligned currents and Alfvén waves by three-dimensional magnetic reconnection, *J. Geophys. Res.*, *104*, 10,177, 1999.

Ma, Z. W., L. C. Lee, and A. Otto, Generation of field-aligned currents and Alfvén waves by 3-D magnetic reconnection, *Geophys. Res. Lett.*, *22*, 1737, 1995.

Nakamura, M., and M Scholer, Structure of the magnetopause reconnection layer and of flux transfer events: Ion kinetic effects, *J. Geophys. Res.*, *105*, 23,179, 2000.

Nakamura, M., et al., Leakage ions from the LLBL to MSBL: Confirmation of reconnection events at the dayside magnetopause, *J. Geomagn. Geoelectr.*, *47*, 65, 1996.

Ogino, T., R. J. Walker, M. Ashour-Abdalla, and J. M. Dawson, An MHD simulation of the effects of the interplanetary magnetic field B_y component on the interaction of the solar wind with the Earth's magnetosphere during southward interplanetary magnetic field, *J. Geophys. Res.*, *91*, 10,029, 1986.

Ohtani, S., T. Higuchi, T. Sotirelis, and P. T. Newell, Disappearance of large-scale field-aligned current systems: Implications for the solar wind-magnetosphere coupling, in *Magnetospheric Current Systems, Geophys. Monogr. Ser.*, vol. 118, edited by S. Ohtani et al., pp. 253-259, AGU, Washington, D. C., 2000.

Omidi, N., and D. Winske, Structure of the magnetopause inferred from one-dimensional hybrid simulations, *J. Geophys. Res.*, *100*, 11,935, 1995.

Omidi, N., H. Karimabadi, and D. Krauss-Varban, Hybrid

simulation of the curved dayside magnetopause during southward IMF, *Geophys. Res. Lett., 25*, 3273, 1998.

Papamastorakis, I., G. Paschmann, W. Baumjohann, B. U. O. Sonnerup, and H. Luhr, Orientation, motion, and other properties of flux transfer evet structures on September 4, 1984, *J. Geophys. Res., 94*, 8852, 1989.

Paschmann, G., B. U. O. Sonnerup, I. Papamastorakis, N. Sckopke, G. Haerendel, S. J. Bame, J. R. Asbridge, J. T. Gosling, C. T. Russell, and R. C. Elphic, Plasma acceleration at the Earth's magnetopause: evidence for reconnection, *Nature, 282*, 243, 1979.

Phan, T. D., et al., Extended magnetic reconnection at the Earth's magnetopause from detection of bi-directional jets, *Nature, 404*, 848, 2000.

Russell, C. T., and R. C. Elphic, Initial ISEE magnetometer results: Magnetopause observations, *Space Sci. Rev., 22*, 691, 1978.

Russell, C. T., P. Song, and R. P. Lepping, The Uranian magnetopause: Lessons from the Earth, *Geophys. Res. Lett., 16*, 1485, 1989.

Russell, C. T., G. Le, and S. M. Petrinec, Cusp observations of high- and low-latitude reconnection for northward IMF: An alternative view, *J. Geophys. Res., 105*, 5489, 2000.

Sato, T., R. J. Walker, and M. Ashour-Abdalla, Driven magnetic reconnection in three dimensions: Energy conversion and field-aligned currents, *J. Geophys. Res., 89*, 9761, 1984.

Saunders, M. A., Origin of the cusp Birkeland currents, *Geophys. Res. Lett., 16*, 151, 1989.

Saunders, M. A., C. T. Russell, and N. Sckopke, Flux transfer events: Scale and interior structure, *Geophys. Res. Lett., 11*, 131, 1984.

Scholer, M., Asymmetric time-dependent and stationary magnetic reconnection at the dayside magnetopause, *J. Geophys. Res., 94*, 15,099, 1989.

Scholer, M., and A. Otto, Magnetotail reconnection: Current diversion and field-aligned currents, *Geophys. Res. Lett., 18*, 733, 1991.

Scudder, J. D., P. Puhl-Quinn, F. S. Mozer, K. Ogilvie, and C. T. Russell, Generalized Walén tests through Alfvén waves and rotational discontinuities using electron flow velocities, *J. Geophys. Res., 104*, 19,817, 1999.

Shay, M. A., J. F. Drake, B. N. Rogers, and R. E. Denton, Alfvénic collisionless magnetic reconnection and the Hall term, *J. Geophys. Res., 106*, 3759, 2001.

Shi, Y. and L. C. Lee, Structure of the reconnection layer at the dayside magnetopause, *Planet. Space Sci., 38*, 437, 1990.

Sonnerup, B. U. O., Magnetic field reconnection, in *Solar System Plasma Physics, Vol. III*, p.45, edited by C. F. Kennel, L. T. Lanzerotti, and E. N. Parker, North Holland Publishing Company, 1979.

Sonnerup, B. U. O., and L. H. Cahill Jr., Explorer 12 observations of the magnetopause current layer, *J. Geophys. Res., 73*, 1757, 1968.

Sonnerup, B. U. O., and B. G. Ledley, OGO 5 magnetopause structure and classical reconnection, *J. Geophys. Res., 84*, 399, 1979.

Sonnerup, B. U. O., G. Paschmann, I. Papamastorakis, N. Sckopke, G. Haerendel, S. J. Bame, J. R. Asbridge, J. T. Gosling, and C. T. Russell, Evidence for magnetic reconnection at the Earth's magnetopause, *J. Geophys., Res., 86*, 10,049, 1981.

Swift, D. W., Use of a hybrid code for a global-scale plasma simulation, *J. Comput. Phys., 126*, 109, 1996.

Swift, D. W., and L. C. Lee, Rotational discontinuities and the structure of the magnetopause, *J. Geophys. Res., 88*, 111, 1983.

Tidman, D. A., and N. A. Krall, *Shock Waves in Collisionless Plasmas*, John Wiley, New York, 1971.

Vasyliunas, V. M., Theoretical models magnetic field line merging, *Rev. Geophys., 13*, 303, 1975.

Wu, B. H., and L. C. Lee, Hall effects on the Walén relation in rotational discontinuities and Alfvén waves, *J. Geophys. Res., 105*, 18,377, 2000.

Xie, H., and Y. Lin, Two-dimensional hybrid simulation of the dayside reconnection and associated ion transport, *J. Geophys. Res., 105*, 25,171, 2000.

Y. Lin, Physics Department, Auburn University, 206 Allison Laboratory, Auburn, AL 36849-5311, USA. (ylin@physics.auburn.edu)

(Received May, 19, 2000; revised June 15, 2001; accepted July 16, 2001.)